

# THREE-BODY CAPTURE OF IRREGULAR SATELLITES: APPLICATION TO JUPITER

Catherine Philpott<sup>1</sup>, Douglas P. Hamilton<sup>1</sup>, and Craig B. Agnor<sup>2</sup>

<sup>1</sup> Department of Astronomy, University of Maryland, College Park, MD 20742-2421

E-mail: [cphilpott@astro.umd.edu](mailto:cphilpott@astro.umd.edu)

[hamilton@astro.umd.edu](mailto:hamilton@astro.umd.edu)

<sup>2</sup> Astronomy Unit, School of Mathematical Sciences, Queen Mary University of London,

London, UK E14NS

E-mail: [c.b.agnor@qmul.ac.uk](mailto:c.b.agnor@qmul.ac.uk)

Submitted to *Icarus*: October 19, 2009

## ABSTRACT

We investigate a new theory of the origin of the irregular satellites of the giant planets: capture of one member of a  $\sim 100$ -km binary asteroid after tidal disruption. The energy loss from disruption is sufficient for capture, but it cannot deliver the bodies directly to the observed orbits of the irregular satellites. Instead, the long-lived capture orbits subsequently evolve inward due to interactions with a tenuous circumplanetary gas disk.

We focus on the capture by Jupiter, which, due to its large mass, provides the most stringent test of our model. We investigate the possible fates of disrupted bodies, the differences between prograde and retrograde captures, and the effects of Callisto on captured objects. We make an impulse approximation and discuss how it allows us to generalize capture results from equal-mass binaries to binaries with arbitrary mass ratios.

We find that at Jupiter, binaries offer an increase of a factor of  $\sim 10$  in the capture rate of 100-km objects as compared to single bodies, for objects separated by tens of radii that approach the planet on relatively low-energy trajectories. These bodies are at risk of collision with Callisto, but may be preserved by gas drag if their pericenters are raised quickly enough. We conclude that our mechanism is as capable of producing large irregular satellites as previous suggestions, and it avoids several problems faced by alternative models.

## 1. Introduction

### 1.1. Previously suggested capture models

With discoveries accelerating in the last decade, we now know of over 150 satellites orbiting the giant planets. About one-third of these are classified as regular, with nearly circular and planar orbits. It is thought that these satellites are formed by accretion in circumplanetary disks. The majority of the satellites, however, are irregular and follow distant, highly eccentric and inclined paths. It is widely believed that irregular satellites originated in heliocentric orbits and were later captured by their planets, but the details of how this occurred are still uncertain. At least seven different models have been proposed, involving dissipative forces, collisions, resonances, and three-body effects. Each model has its own strengths and weaknesses.

In one long-standing theory, planetesimals are slowed as they punch through the gas disk surrounding a young, growing planet (Pollack *et al.*, 1979). For this mechanism to be efficient, the gas must be sufficiently dense to capture the planetesimals in one pass. This is problematic, however, because if the gas disk does not rarefy substantially in  $\sim 100$ - $1000$  years, the orbits of the new satellites will decay inward, leading to collisions with the planet and its regular satellites. Furthermore, the atmospheres of Uranus and Neptune have only a few Earth-masses of hydrogen and helium at present, so their gas disks could not have been as extensive or long-lived as those of Jupiter and Saturn. A likely outcome of this model, then, is that satellite capture should have been different at Jupiter and Saturn than

at Uranus and Neptune; however, current observational estimates suggest equal efficiencies (Jewitt & Sheppard, 2005). With a model similar to that of Pollack *et al.*, Čuk & Burns (2004a) found that Jupiter’s largest irregular satellite, Himalia, would evolve inward to its current orbit in  $10^4 - 10^6$  years. This tenuous gas, however, may make capture difficult.

In another model, planetesimals are captured when the mass of the planet increases (Heppenheimer & Porco, 1977). This mass growth causes the planet’s escape velocity to increase, rendering a previously free planetesimal bound to the planet. For this method to be effective, the planet’s mass must increase substantially on  $\sim 100$ - $1000$ -year timescales. However, in most planet formation models (e.g. Pollack *et al.*, 1996), giant planet growth is hypothesized to take place on timescales many orders of magnitude longer than required by this capture scenario. Furthermore, Uranus and Neptune’s gas deficiency implies that their growth was of very short duration. Thus, our current understanding of planetary formation makes this model improbable.

The observation that the four giant planets contain approximately the same number of irregular satellites (accounting for observational biases; Jewitt & Sheppard, 2005) has led to a renewal of interest in capture theories that do not depend strongly on the planet’s formation process. In one such scenario, a planetesimal collides with a current satellite or another planetesimal in the vicinity of the planet, resulting in its capture (Colombo & Franklin, 1971). Though collisions were certainly more common in the early Solar System than they are today, if they resulted in enough energy loss to permit capture, they would

likely also have catastrophically disrupted the bodies. Nevertheless, the fragments might then have become independent satellites.

A fourth suggestion involves the possible instability in the orbits of the outer planets early in the Solar System (e.g., by a 2:1 resonance crossing between Jupiter and Saturn). Outlining the theory of the Nice model of Solar System evolution, Tsiganis *et al.* (2005) have shown that such an event could cause Uranus and Neptune to have many close approaches with each other and with Jupiter and Saturn. During these encounters, the influence of the massive interloping planet can cause planetesimals to be stabilized as satellites (Nesvorný *et al.*, 2007). This method is promising but has an important disadvantage in that Jupiter (and Saturn, to a lesser extent) sustains very few close encounters relative to the ice giants. Thus the gas giants are inefficient at capturing satellites in this way (Nesvorný *et al.*, 2007).

Astakhov *et al.* (2003) examined low-energy orbits that linger near Jupiter and Saturn. While these bodies are not permanently captured, the authors found that some of them were stable for thousands of years, long enough to allow a weak dissipative force such as gas drag to complete the capture process. However, the overall percentage of temporary captures that do not escape is small, and many of these bodies are threatened by collision with the planets' large outer satellites (e.g., Callisto and Titan).

Agnor & Hamilton (2006a) examined the capture of Triton from an exchange reaction between a binary pair and Neptune. Their motivation stemmed from the newly-discovered abundance of binaries in small-body populations. Currently, it is estimated that binaries

account for  $\sim 30\%$  of Kuiper belt objects (KBOs) with inclinations  $< 5^\circ$ ,  $\sim 5\%$  of the rest of the KBOs (Noll *et al.*, 2008), and  $\sim 2\%$  of large main belt asteroids (diameters  $> 20$  km; percentage increases for smaller objects; Merline *et al.*, 2007). In Agnor & Hamilton’s capture model, a binary is tidally disrupted and one of its members, Triton, is captured as a satellite. This process is most effective for large satellites like Triton, with radius 1350 km. However, the largest of the other irregular satellites are more than 10 times smaller than Triton: Himalia at Jupiter is  $\sim 85$  km in radius, Saturn’s largest irregular, Phoebe, is  $\sim 110$  km, Uranus’s Sycorax is  $\sim 80$  km, and Neptune’s Halimede and Neso are only  $\sim 30$  km each. Capturing these satellites via binary exchange reactions would be significantly more difficult, as we will discuss further below.

Finally, Vokrouhlický *et al.* (2008) examined binary exchange reactions during the first 100 Myr after an assumed Jupiter/Saturn 2:1 resonance crossing, using results of the Nice model (Tsiganis *et al.*, 2005) to guide their initial conditions. Because planetesimal speeds relative to the planets are high after the scattering phase of the Nice model, they found that captures from binaries during that time do not match current orbital parameters and occur too infrequently to account for today’s populations.

## 1.2. Our model: Capture from 100-km binaries

All of the above models have promising aspects coupled with important limitations. In this work, we seek to combine the best features of several models into a viable capture sce-

nario. In particular, we examine binaries (as in Agnor & Hamilton, 2006a and Vokrouhlický *et al.*, 2008) as a way to augment capture from low-velocity orbits resulting from three-body interactions like those studied by Astakhov *et al.* (2003). While Vokrouhlický *et al.* (2008) studied exchange reactions in the context of an assumed initial planetesimal population, we focus on assessing the viability of the mechanism itself. Our goal is to determine how various parameters of the model affect its plausibility. We examine its viability at Jupiter, as a number of the above models suggest that capturing at the largest gas giant is especially difficult.

As the largest of the existing irregular satellites are  $\sim 80$ - $110$  km, capture of objects in this size-range is particularly interesting. Since it is likely that the irregular satellite population contains collisional families (Nesvorný *et al.*, 2003; Sheppard & Jewitt, 2003), it may be the case that only the largest objects were captured, while the smaller satellites formed later, via collisions. For this reason, we focus our investigation on capturing the  $\sim 100$ -km progenitors.

In order to stabilize and shrink the resulting capture orbits, a dissipation source is required; we suggest a tenuous version of the gas drag originally proposed by Pollack *et al.* (1979). Two of Jupiter’s irregular satellites, Pasiphae and Sinope, as well as Saturn’s satellite, Siarnaq, and Uranus’ Stephano, are found in resonances that seem to require just such a weak dissipative force (Whipple & Shelus, 1993; Saha & Tremaine, 1993; Čuk & Burns, 2004b).

Furthermore, a tenuous circumplanetary disk is consistent with current theories of late-stage planetary formation. Jupiter’s massive gaseous envelope of hydrogen and helium necessitates that it formed in the Solar System’s circumstellar gas disk. Before the end of its accretion, Jupiter was likely able to open a gap in the local density distribution of the gas (for a review, see e.g. Papaloizou *et al.*, 2008). After gap opening, gas continues to leak into the planet’s Hill sphere through the  $L_1$  and  $L_2$  points, but at a rate much reduced in comparison to the previous epochs. A tenuous circumplanetary gas disk results (e.g., Lubow *et al.*, 1999; D’Angelo *et al.*, 2003; Bate *et al.*, 2003), from which material may condense and regular satellites may accrete near the planet (e.g., Canup & Ward, 2002; Mosquera & Estrada, 2003).

In Ćuk & Burns’ study (2004a) of the Himalia progenitor’s orbital evolution, they considered circumjovian nebular conditions consistent with hydrodynamical simulations of Jupiter’s gap opening in a circumstellar gas disk (e.g., Lubow *et al.*, 1999) and found that the post-capture timescale for evolving this progenitor to its present orbit to be roughly in the range of  $10^4 - 10^6$  years. This is similar to the timescale in which extrasolar circumstellar disks transition from optically thick to thin ( $\sim 10^5$  years; Skrutskie *et al.*, 1990; Silverstone *et al.*, 2006; Cieza *et al.*, 2007). The similarity of timescales suggests that satellites captured at the onset of disk dispersal have a good chance of experiencing stabilizing orbital evolution while also avoiding collision with the planet.

The timescale for binary capture is very short compared to evolution timescales from

a tenuous gas disk. Therefore, we focus our study first on characterizing the effectiveness of binary capture in the absence of gas. In the following sections, we critically evaluate our model for capturing irregular satellites from low-mass ( $\sim 100$ -km) binaries. We begin with a closer examination of the three-body capture process and then explore parameter space with a large suite of numerical simulations. We then discuss the ability of gas drag to stabilize post-capture orbits in Section 4.7.

## 2. Three-body capture process

Binary capture first requires a close approach between a binary pair and a planet. As the pair approaches the planet on a hyperbolic trajectory, its two components also orbit their mutual center of mass (CM). Hence, each member’s speed with respect to the planet is a vector sum of its CM speed ( $v_{CM}$ ) and its orbital speed around the CM. If the binary passes close enough to the planet, it will be tidally disrupted. Following Agnor & Hamilton (2006a), we make an ‘impulse approximation’ and assume that disruption is instantaneous, so that the distance at which tidal disruption occurs ( $r_{td}$ ) can be estimated as:

$$r_{td} \approx a_B \left( \frac{3M_P}{m_1 + m_2} \right)^{1/3}, \quad (1)$$

where  $a_B$  is the semi-major axis of the binary,  $M_P$  is the mass of the planet, and  $m_1$  and  $m_2$  are the masses of the binary pair. This tidal disruption radius is the distance to the planet at which the binary’s Hill sphere is no longer larger than the binary itself.

As a result of the impulse approximation, we also assume the orbits of the now-separated components are dictated by their speeds upon disruption. The speed change of one component ( $\Delta v_1$ ) is approximately equal to its orbital speed around the CM:

$$\Delta v_1 \approx \pm \frac{m_2}{m_1 + m_2} \left( \frac{G(m_1 + m_2)}{a_B} \right)^{1/2}, \quad (2)$$

where  $G$  is the gravitational constant. If the speed of either component is below the escape speed ( $v_{esc}$ ) when the binary is split, that component will be captured. This is most efficient if the incoming  $v_{CM}$  is only slightly faster than the value needed for escape. (See Fig. 1.)

The separation of the binary ( $r_B = 2a_B$ , for equal-mass pairs on circular orbits) plays a key role in determining whether a given encounter will result in a capture. From Eq. 2, we can see that a smaller separation imparts a higher speed change upon disruption, increasing the probability of capture. However, the separation must be large enough that the binary can actually be disrupted. Equation 1 indicates that, not surprisingly, a large separation makes the binary easier to split. The separation that optimizes capture, then, is one just wide enough that the binary is disrupted. In addition, the tidal radius is important: the speed change needed for capture ( $v_{CM} - v_{esc}$ , the difference between the two horizontal lines in Fig 1) decreases for smaller  $r_{td}$ . Thus deeper encounters are more likely to lead to captures.

In much of the current work, we consider the simplified case where Jupiter orbits the Sun along a circle. In this case, the Jacobi constant ( $C_J$ ) for the planet-Sun-interloper three-body problem is a very useful predictor of the interloper's potential for capture, taking on the

role of  $v_\infty$  from the two-body approximation. Although our model contains four bodies, and the Jacobi constant is a three-body construct, it is an excellent approximation to consider the CM of the binary as one body moving in the Sun-Jupiter system up until the point of disruption. The gravitational energy between the binary components is negligible after they separate. Thus after disruption, we essentially have two separate three-body problems, one for each binary component, and we can make use of the Jacobi constant throughout the entire simulation.

If  $C_J \geq C_{J,crit}$ , the critical value for capture, bodies in the vicinity of the planet are bound by so-called zero-velocity curves (ZVCs) that enclose Jupiter and constrain particle motions (Fig. 2). For Jacobi constants lower than  $C_{J,crit}$  (i.e., higher energies), one large zero-velocity curve surrounds both Jupiter and the Sun and bodies can enter and exit Jupiter’s Hill sphere freely. The critical Jacobi constant represents the boundary between these possibilities. Murray & Dermott (1999) give its value:  $C_{J,crit} \approx 3 + 3^{4/3}\mu^{2/3} - 10\mu/3$ , where  $\mu = \frac{M_P}{M_\odot + M_P}$  and  $M_\odot$  and  $M_P$  are the masses of the Sun and the planet, respectively. Here we use dimensionless units in which  $G$ , the Jupiter-Sun distance, and the sum of the solar and jovian masses are equal to 1. For the Jupiter-Sun system, which is the focus of the current paper,  $\mu = 9.53 \times 10^{-4}$  and  $C_{J,crit} \approx 3.0387$ .

Figure 3 illustrates a typical capture involving Jupiter. In the bottom panel, the Jacobi constant of the binary pair prior to its split is lower than the critical value, meaning that initially, the binary has too much energy to be bound. The oscillations in the bodies’ pre-

disruption  $C_J$  are due to gravitational interactions between the binary components. At the time of disruption ( $t \approx 8$  yr), one component sharply gains energy ( $C_J$  decreases), while the other component experiences a corresponding energy loss ( $C_J$  increases). In this example, one component’s final  $C_J$  is higher than the critical value, signifying that it is permanently bound to Jupiter. Though the Jacobi constant is very valuable when considering a circularly-orbiting Jupiter, a disadvantage is that it cannot be extended to cases with non-zero eccentricity. In this paper, we make the simplifying assumption that  $e_J = 0$  (rather than the true value of  $\sim 0.048$ ) in order to better elucidate important physics of the problem.

In Fig. 4, we plot the orbits of the binary components shown in Fig. 3. Low-velocity orbits like these are characterized by multiple close passes by the planet (cf. Hamilton & Burns, 1991). The separation is disturbed by the strong tidal force during each of these passes, but the binary splits only after it comes within the tidal disruption radius (see top and middle panels of Fig. 3).

The binary capture mechanism is most effective at producing permanent or long-lived captures if i) the mutual orbital speed of the binary is high, and/or ii) the encounter speed is low. Agnor & Hamilton’s (2006a) work examined Neptune’s moon Triton, which is somewhat of a special case because it fulfills both of these criteria – its size means that its orbital speed around a close companion would be high, and typical encounter speeds at Neptune in the early stages of planet formation are relatively low.

The direct three-body capture mechanism is much less effective for most other irregular

satellites which are  $\sim 100$  km or smaller in radius. Furthermore, because of Jupiter and Saturn’s sizes and proximity to the Sun, encounter speeds at the semi-major axes of the gas giants’ irregular satellites are relatively fast,  $v_{CM} \approx 3$  km/s. To produce a large enough energy change for capturing directly to the current satellites’ locations, binary components must be orbiting each other at speeds comparable to their encounter speeds. This would require binary companions of order Mars- or Earth-sized (Agnor & Hamilton, 2006b) – an uncommon occurrence even in the early Solar System.

Accordingly, in this work, we relax the requirement that moons are captured directly to their present orbits. In the example discussed above (see Fig. 4), the final orbit of the captured satellite extends almost to the Hill radius ( $r_H$ ), whereas the actual satellites at Jupiter are significantly more tightly bound. We investigate the idea that the objects were first captured to these distant orbits, and a subsequent period of orbital evolution (e.g., by weak gas drag) led them to their current configurations.

The post-capture evolution is a key component in our model because it allows for capture from small binary pairs, even though they deliver satellites to very distant orbits. Binaries with primaries of order 100 km were certainly much more numerous than those with planet-sized primaries, even in the early Solar System. Models that rely on gas drag for capture (e.g. Pollack *et al.*, 1979) require both i) dense gas (to enable capture) and ii) rapid dispersal (to prevent satellite loss to the planet). By contrast, our model requires no gas for capture and puts only weak constraints on gas required for orbital evolution. In particular, we require

only that the product of the gas density and its residence time around Jupiter be large enough that the requisite amount of evolution can occur.

### 3. Numerical model

The goal of this work is to characterize the overall effect of binaries on the probability of capturing bodies on planet-crossing paths. We focus primarily on captures at Jupiter, which has the most irregular satellites and has many sources of small bodies nearby. Also, as discussed above, capture at Jupiter has shown to be difficult, especially because of its large size and fast encounter speeds for approaching bodies. Thus these simulations provide the most stringent test of our model.

Our integrations include the Sun, Jupiter, and a binary or single object, in a planet-centered frame. In order to examine binaries' effectiveness at producing long-lived captures, we compare them to captures of single-body interlopers. While only tidally disrupted binaries can be captured permanently, unbound single bodies can remain near the planet for long periods of time (e.g. Astakhov *et al.*, 2003). We define a 'capture' to be a body that remains near Jupiter for 1,000 years, the duration of each simulation. Furthermore, we define 'binary capture' to mean capture of one or both of the bodies that originated together as binary components. Note that these definitions encompass both permanent (energetically bound) and long-lived temporary captures. With captures of single bodies as a baseline, we are able to measure the enhancement due to binaries.

Our simulations are performed with HNBody, a hierarchical  $N$ -body integration package, and HNDrag, a companion code for applying non-gravitational forces to the particles and for detecting close approaches (Rauch & Hamilton, 2002). For most of this work, we use only the close-approach detecting capabilities of HNDrag and include only gravitational forces. We use HNBody’s Bulirsch-Stoer integrator with a specified accuracy of one part in  $10^{14}$ . The adaptive-stepsize Bulirsch-Stoer integrator is much more efficient than a symplectic integrator here because while a small stepsize is needed initially to resolve the orbital motion around the binary CM, it can be greatly increased after disruption.

We ran about 200 sets of three- or four-body simulations examining a range of Jacobi constants for each interloper (2.95-3.037), as well as varying the binaries’ radii (65-, 100-, and 125-km), and separations (1-1000 body radii). For each set of parameters, we generated 10,000 binaries or single objects, for a total of  $\sim 2 \times 10^6$  simulations, each following the bodies for 1,000 years. We started all of the interlopers of a given set at the same distance from the planet, ranging from 1.0 - 1.4  $r_H$ . (Section 4.4 contains a discussion of the effects of starting distances on capture statistics.) The choice of Jacobi constant and starting distance constrains the possible initial positions of the binary CM. Fig. 2 shows Jupiter’s Hill sphere overplotted with ZVCs corresponding to the Jacobi constants that we studied. Bodies are energetically unable to cross their zero-velocity surfaces, and thus starting with, say,  $C_J = 3.037$  at 1.0  $r_H$  from the planet restricts the body’s initial position to the two small ‘endcaps’ of the Hill sphere along the Jupiter-Sun line. For smaller  $C_J$ , these allowed areas are larger and finally encompass the entire Hill sphere for  $C_J \lesssim 3.025$ . The bodies’ initial speeds are

also constrained by the specified Jacobi constant, and we choose the velocity to point in random inward directions.

For simplicity, we set the binary components to orbit each other on circles and the binary angular momentum to be perpendicular to Jupiter’s equatorial plane. We ran each initial condition with five different binary orbital phases (equally-spaced mean anomalies) and averaged all capture statistics over the five phases. Throughout the simulations, we monitored the bodies, weeding out very close approaches between any two objects and noting each body’s close approaches to Jupiter. (Collisions between binary members do occur, but these are rare and of limited interest, since the merged object simply behaves as a single interloper with the same CM speed.) To shorten the computational time required, we stopped integrations in which all of the incoming objects traveled further than 2-5 Hill radii from Jupiter, depending on the bodies’ starting distance from the planet.

## 4. Results

### 4.1. Relationship between inclination and $C_J$

In our simulations, we find that the inclination of the approach trajectory is correlated with the initial Jacobi constant, which is helpful in providing physical intuition for the meaning of  $C_J$ . This correlation was first noticed numerically by Astakhov *et al.* (2003); here we confirm their finding numerically and provide an analytical explanation. Fig. 5 displays this  $C_J$ -inclination relationship. We see a clear correlation of  $C_J$  with mean inclination:

lower Jacobi constants are indicative of retrograde orbits, while prograde orbits have larger  $C_J$ . For clarity, the plot shows only a representative population of bodies: 100-km binary members that result in a capture, with inclinations calculated at the closest approach of each body’s first pass by Jupiter. However, the relationship holds for all close approaches of binaries or single objects, captured or not. This plot provokes two main questions: what is the physical cause of this trend and why is there such high scatter in inclination at a given Jacobi constant? We address the question of scatter first.

One complexity in making this plot is that all orbital elements including inclination are poorly defined at large distances from Jupiter, as solar tides are comparable to Jupiter’s gravity at the Hill sphere. Accordingly, we were careful to calculate the inclinations only at orbital pericenter where solar tides are weakest so that inclination is always well defined. Poorly-defined orbital elements, therefore, are not the source of the scatter. Furthermore, the variations look nearly the same when we plot single objects rather than binaries, which is expected since disrupting the binary results in an energy change that only slightly alters  $C_J$  (e.g., Fig. 3). Finally, the scatter is present even when we consider one individual object’s multiple pericenter passages rather than those of an ensemble of objects. Thus the spread in inclination is real and is due to the response of a single captured object to the solar tidal force.

The scatter in inclination as well as the inclination- $C_J$  trend can be understood analytically by writing the Jacobi constant in terms of planetocentric orbital elements rather than

the heliocentric orbital elements used in deriving the standard Tisserand constant (Murray & Dermott, 1999). We begin with the planet-centered ‘generalized Tisserand constant’ derived in Hamilton & Krivov, 1997 (their Eq. 4) and neglect the solar tidal term since it is complicated and unimportant at pericenter where we measure inclination. We then non-dimensionalize the equation as described in Section 2, and finally, to conform to standard usage (Murray & Dermott, 1999), we add the constant 3 to the final result and find:

$$C_{J'} = 3 + \frac{3^{1/3}\mu^{2/3}}{\bar{a}} \left[ 1 + 2 \left( \frac{\bar{a}^3(1-e^2)}{3} \right)^{1/2} \cos(i) \right], \quad (3)$$

where  $\mu$  is the mass ratio as defined above;  $\bar{a} = a/r_H$ ; and  $a$ ,  $e$ , and  $i$  are the captured satellite’s semi-major axis, eccentricity, and inclination, respectively. Because we have neglected the solar tidal term and used planetocentric orbital elements, this expression is valid only near the planet where solar perturbations are weak.

For close orbits of the planet ( $\bar{a} \ll r_H$ ), orbit-averaging the effects of the tidal force shows that the semimajor axis  $\bar{a}$  remains constant. Accordingly, Eq. 3 leads directly to the Kozai constant,  $K = \sqrt{1-e^2} \cos(i)$ . This constant explains the coupled oscillations in eccentricity and inclination that characterize the Kozai resonance. If  $K$  were precisely conserved, orbits would not be able to switch between  $i < 90^\circ$  (which have  $K > 0$ ) and  $i > 90^\circ$  (which have  $K < 0$ ). We do, however, see such prograde-to-retrograde transfers in Fig. 5, which indicates that, as expected,  $K$  (and therefore  $\bar{a}$ ) is not constant for our distant orbits (see, e.g., Hamilton & Burns, 1991). In addition, at apocenter where the

solar tidal force is strongest, the orbital elements themselves are poorly defined and Eq. 3 is only approximate. Thus between each pericenter passage, the orbital elements (including inclination) are scrambled by the solar tidal force leading to dispersion like that seen in Fig. 5.

The trend observed in Fig. 5, decreasing inclination for increasing Jacobi constant, is neatly explained by Eq. 3. Testing the equation quantitatively, we estimate  $\bar{a} = 0.5$  and  $e = 0.7$  for a typical orbit of a body captured at Jupiter (e.g., Fig. 4). A purely prograde orbit ( $i = 0$ ) gives  $C_J' = 3.036$ , while a purely retrograde orbit ( $i = 180^\circ$ ) gives  $C_J' = 3.020$ . These values roughly correspond to the range of Jacobi constants seen in Fig. 5, despite the rather large approximations that we have made. The inclination- $C_J$  correlation is strong enough that we will often use the term prograde to refer to orbits with  $C_J \sim 3.03$ , and retrograde to mean  $C_J \sim 3.01$ .

## 4.2. Modes of capture

For each binary-planet encounter, there are four possible outcomes: (1) neither component captures (hereafter known as '0C'), (2) one component captures ('1C'), (3) both components capture together as an intact binary without splitting apart ('2C-BIN'), or (4) the binary is disrupted and both components capture individually ('2C-IND'). The frequency of each type of outcome depends on the characteristics of the binary. Fig. 6 shows the outcomes that result in a capture (i.e., 1C, 2C-BIN, and 2C-IND) for 65-km binary pairs with

initial  $C_J = 3.037$ , as a function of the initial separation,  $r_B$ , of the binary. The separation can be altered significantly prior to disruption during close approaches to the planet. The number of captures for a set of single objects is also plotted for comparison; these must be temporary captures since there is no energy loss.

The rate of 2C-BIN captures is largest when the separation is small (and thus the components are tightly bound to each other). For small-enough separations, the tidal disruption radius is so close to the planet that very few binary orbits cross it (see Eq. 1). Here, most of the binaries remain intact, and the 2C-BIN rate nearly matches that of single objects. When we increase the binary separation, more binaries are split, and the 2C-BIN capture percentage monotonically drops to zero, as expected.

Disrupting binaries leads to more possibilities for capture of individual objects. Accordingly, as the separation increases, the 1C and 2C-IND capture rates rises from zero. For the 1C population of 65-km objects with  $C_J = 3.037$ , there is a peak in capture efficiency of  $\sim 5$  times that of a single body at a separation of  $\sim 20$  body radii ( $R_B$ ). This separation represents the optimal balance between disrupting a high percentage of the binaries and delivering the most energy upon disruption. The optimum separation varies depending on the mass of the binary. At larger separations, the binding energy decreases, leading to smaller energy kicks and a diminished capture rate.

The 2C-IND percentage has a peak at the same separation as the 1C group. These binaries likely split during orbital phases where the energy is distributed almost equally

between the components. The number of 2C-IND captures is never more than a few percent of the 1C captures, but the two populations peak at  $r_B \sim 20 R_B$  for the same reasons. More widely separated binaries are disrupted with a smaller energy change. Because of this, the two components are more likely to have similar energies and post-disruption fates, causing an increase in 2C-IND captures at larger separations.

Unlike the case for 1C and 2C-IND capture where energy is lost and capture can be long-lived or even permanent (as in Fig. 3), capture of singles or intact binaries (2C-BIN) is necessarily temporary. This could be an advantage for 1C captures, which have more stable, lower-energy initial capture orbits. The details of the final comparative satellite yields depend on the subsequent orbital evolution, which is determined by the gas present at the time of capture and its dissipation timescale.

### 4.3. Effects of binary mass and orbital separation

Having explored the physical meaning of  $C_J$  and the possible types of captures, we now discuss the results of the numerical simulations. In this section, we consider cases of equal-mass binaries encountering Jupiter with the planet on a circular orbit, and we examine the effects of the bodies' masses, binary separations, and initial Jacobi constants. We performed integrations over a range of Jacobi constants:  $2.95 \leq C_J \leq 3.037$ , where  $C_J \approx 3.0387$  is the critical value above which transfer orbits between Jupiter and the Sun are impossible (see Fig. 2). For  $C_J \leq 2.99$ , no captures resulted for any of the parameters we tested, although

capture at these low Jacobi constants could certainly occur for larger-mass binaries. For now, we consider the fate of bodies started from the Hill sphere (following Astakhov *et al.*, 2003); in Section 4.4, we discuss the importance of alternative starting distances.

We examined masses corresponding to pairs of objects each with radii 65-km, 100-km, and 125-km (assuming a density of  $\sim 2 \text{ g/cm}^3$ ). Fig. 7 displays the results of these mass studies. We see that capture rates increase for higher masses: the 125-km capture rate is slightly higher than the 100-km rate throughout the range of Jacobi constants, and they differ most significantly from 65-km binary pairs for  $C_J > 3.03$ .

For single objects, mass has no effect on capture probability, but for binaries, larger total mass leads to more rapid orbital speeds and a higher speed change upon breakup. This can be seen by eliminating  $a_B$  from Eqs. 1 and 2, with mass ratio ( $\frac{m_2}{m_1+m_2}$ ) and tidal distance ( $r_{td}$ ) held constant; the result is  $\Delta v_1 \sim (m_1 + m_2)^{1/3}$ . Accordingly, larger masses generally lead to increased capture rates.

Another important result is that capture rates from binaries are extremely sensitive to the binary’s separation,  $r_B = 2a_B$ . For each of the masses we examined, we determined the optimum separation of the binary required to achieve the maximum capture probability. We used Eqs. 1 and 2 to guide our separation selection, and we integrated each point on Fig. 7 with several different binary separations to determine the optimal value.

In Fig. 7, we have plotted statistics using a single separation for each mass over the range of Jacobi constants. For most of the Jacobi constants studied for a given mass, the

optimal separations are very similar,  $\sim 10 R_B$ . An important exception is for the highest  $C_J$  value tested, 3.037 (recall that this corresponds to mostly prograde encounters – see Fig. 5), which had maximum captures at a larger separation ( $\sim 20 R_B$ ) than the typical optimal value. Because we have not plotted this optimal value in Fig. 7, the curve declines sharply at  $C_J = 3.037$ . As is clear from Section 4.2, optimizing the separation makes a significant difference in capture rate, especially for binaries whose  $C_J$  values are close to the capture threshold. Changing from  $\sim 10 R_B$  to the optimal  $20 R_B$  for  $C_J = 3.037$  increases the capture percentage from  $\sim 2\%$  to  $\sim 10\%$  (100-125 km objects) and  $\sim 1\%$  to  $\sim 3\%$  (65-km, see Fig. 6).

Binary capture rates also appear to depend strongly on initial Jacobi constant. It is tempting to compare capture efficiencies for low and high Jacobi constants (retrograde and prograde orbits). A direct comparison of these rates, however, cannot be made for reasons that will become apparent in the next section. We can, however, compare the binary statistics to those of single objects. The bodies that originate in binaries capture with similar rates as the single objects below  $C_J \approx 3.015$ , but as  $C_J$  increases, the effects of the binaries become more visible, rising by an order of magnitude in efficiency at delivering objects to Jupiter. Part of the reason for this is probably that the retrograde binaries are harder to split than progrades because of their orientation to the planet. Another explanation, particularly for the highest initial Jacobi constants, is that these encounters are close to the critical energy barrier for capture, and so the energy change from disruption of the binary is more likely to result in capture.

#### 4.4. Effects of starting distance

##### 4.4.1. Contamination from bound retrograde orbits

Thus far we have discussed results from initial conditions that launch objects from the Hill sphere. In the course of this study, we discovered that the choice of starting distance can significantly affect the capture statistics. While the Hill sphere is defined as a rough stability boundary beyond which the Sun’s gravitational influence is stronger than the planet’s, in practice, stable retrograde orbits can extend out to distances slightly beyond the Hill radius (see, e.g., Hamilton & Burns, 1991). In contrast, stable prograde orbits (e.g., Fig. 4) are always well within the Hill sphere. Starting the integrations with bodies on the Hill sphere, then, risks starting on an already-stable retrograde orbit. This causes ambiguity in the capture statistics – which orbits were always near Jupiter and which truly came in from infinity?

We demand that true captures originate in heliocentric orbit and transition to planet-centered orbits, remaining for at least 1,000 years. To differentiate between these and misleading ‘captures’ from bodies that are already orbiting the planet at the beginning of our integration, we took the single-body capture orbits and integrated the initial conditions backwards in time for 1,000 years. We then separated the captures that came in from infinity and those that were always present near the planet. We found that when starting on the Hill sphere, most of the resulting retrograde captures of single objects at low  $C_J$  had always been orbiting the planet and were in fact not true captures.

We examined several other launch distances and determined that starting from 1.1 Hill radii ( $r_H$ ) and beyond eliminates nearly all contamination from already-stable retrograde orbits. Figure 8 compares the capture rates for single objects beginning from 1.0  $r_H$  and 1.1  $r_H$ . We see that while the high- $C_J$  captures are uncontaminated, launching from 1.0  $r_H$  for  $C_J < 3.03$  leads to many false captures. In fact, over one-third of the 1.0  $r_H$  captures are contaminations. (This fraction is much smaller for binaries, where there are many more prograde captures than retrograde.) When the objects are launched from 1.1  $r_H$ , we see no artificial captures at all. Similar tests at 1.2  $r_H$  and 1.4  $r_H$  also show no false captures. Although stable orbits do exist to these and larger distances (Henon, 1969), they are apparently extremely rare.

#### 4.4.2. *Scaling to different starting distances*

So, is it safe to compare prograde and retrograde capture statistics for starting distances beyond 1.1  $r_H$ ? Starting outside the Hill sphere results in a decrease in true captures over the full range of  $C_J$  (as seen in Fig. 8). This is expected, because fewer of these bodies experience close approaches with the planet. However, prograde captures are more drastically reduced than retrogrades. Determining the reason for this is critical to answering our question.

At high Jacobi constants ( $\gtrsim 3.03$ , which correspond to mostly prograde orbits), the binary’s ZVCs are closed around the planet except for only a small neck on either side of Jupiter, toward and away from the Sun (see Fig. 2). In contrast, lower Jacobi constants

(and thus retrograde orbits) allow for more freedom of movement in the region between the Sun and Jupiter. Retrograde orbits can approach the planet from all directions, while progrades are limited to the entering via the narrow ZVC necks. Starting further than the Hill sphere means that a smaller fraction of the initial prograde trajectories pass through the zero-velocity necks and approach Jupiter, resulting in a decrease in captures. We tested the hypothesis that the shape of the prograde ZVCs is the primary reason for the decrease in prograde captures with the following procedure:

- 1) Determine the capture rate at  $1.2 r_H$ .
- 2) Determine the crossing rate of  $1.2 r_H$  orbits inside  $1.1 r_H$ .
- 3) Scale the  $1.1 r_H$  capture rate by the crossing rate from step (2).

We use the statistics for  $1.1 r_H$  and  $1.2 r_H$  because they are free from any contamination from the false retrograde captures discussed above. The result of step (3) is what we expect the  $1.2 r_H$  capture percentages would be if the ZVC shapes are the reason for the decline in prograde captures from  $1.1 r_H$  to  $1.2 r_H$ . Comparing these scaled capture rates with the actual  $1.2 r_H$  percentages (as shown in Fig. 9), we see that this scaling accounts for most of the difference between the two capture rates, to within 20%. This indicates that our prediction is valid.

In principle, these results also account for the reduction in true retrograde captures, but the number statistics are so low for retrogrades at these launch distances that the actual and scaled capture percentages are equivalent to within the error.

We find, then, that because of the differing geometries of their ZVCs, we cannot directly compare prograde and retrograde statistics. This is true even when starting beyond the limit for already-stable retrograde orbits, chiefly because prograde orbits are so sensitive to their initial distance. To circumvent this effect, we would have to start far enough away from the planet that further increasing the starting distance would result in an equal fractional decrease in captures for retrogrades and progrades – in other words, where the geometry of the prograde ZVCs is no longer the dominant reason for the decrease. Our simulations, out to  $1.4 r_H$ , did not reach this threshold and were limited by number statistics. We anticipate that comparing prograde and retrograde captures would require starting still further from the planet than our trials, and would demand much larger initial populations.

#### 4.4.3. *Starting from $1.1 r_H$ vs. $1.0 r_H$*

Launching binaries from  $1.1 r_H$  rather than  $1.0 r_H$  results in an overall decrease in captures for the reasons described above, but many of the characteristics of the capture orbits remain relatively unchanged. For example, the inclination distribution for the  $1.1 r_H$  captures is almost identical to the  $1.0 r_H$  population plotted in Fig. 5. Also, comparing Fig. 9 with Fig. 7, we see that the trend in the capture percentage with  $C_J$  of the 100-km binaries at  $1.1 r_H$  and  $1.0 r_H$  are generally similar.

Figure 10 displays the modes of capture vs. Jacobi constant for 100-km binaries and single objects starting from both  $1.0 r_H$  and  $1.1 r_H$ . Starting at  $1.1 r_H$  results in a depletion

of 2C captures relative to 1C captures. This is because many of the retrograde 2C-IND and 2C-BIN captures were likely the artificial retrogrades which are eliminated when starting from  $1.1 r_H$ . The single captures also appear depleted relative to the other curves, but in fact, the binaries are diminished by a roughly comparable amount. Overall, there are few qualitative differences between the  $1.0 r_H$  and the  $1.1 r_H$  cases.

We note that other groups (including Astakhov *et al.*, 2003 and Astakhov & Farrelly, 2004) have initiated bodies from the Hill sphere without considering how this affects the resulting statistics, most notably that many of their retrograde encounters are started on already-stable orbits. For future studies of capture near Jupiter, we recommend the following procedure: 1) generate bodies starting from  $1.0 r_H$ , 2) integrate each body backwards in time, 3) eliminate those that remain near the planet when integrated backwards, and 4) integrate the remaining bodies in normal time direction. The benefits of this approach over simply starting from  $1.1 r_H$  are that it eliminates all stable-retrograde contamination while preserving high number statistics. Note, however, that this procedure still does not allow a valid comparison between prograde and retrograde statistics. To obtain the true ratio of captured progrades and retrogrades, it would probably be best to start the interlopers on heliocentric orbits.

#### 4.5. Scaling to unequal binary masses

The impulse approximation (Eqs. 1 and 2) implies that a binary component’s likelihood of capture depends only on 1) the binary’s tidal disruption radius and 2) the component’s instantaneous speed at the time of disruption. Accordingly, for any mass ratio  $m_1 : m_2$  and semi-major axis  $a_B$ , we can find an equal-mass binary with the same  $r_{td}$  and the same component speeds as  $m_1$  and another equal-mass binary that matches these values for  $m_2$ . Setting  $r_{td}$  and  $v$  equal for the two mass ratios, we solve for the component mass,  $m'$ , and the semi-major axis,  $a_B'$ , of the equal-mass binary matching  $m_1$ :

$$m' = \frac{4m_2^3}{(m_1 + m_2)^2} \quad (4)$$

and

$$a_B' = a_B \left( \frac{2m_2}{m_1 + m_2} \right). \quad (5)$$

The problem is symmetric, so for the equal-mass binary matching  $m_2$ , we simply exchange  $m_1$  and  $m_2$  in the above equations.

We tested these predictions for 3:2 and 4:1 mass ratios and display the results in Table 1. Each of the equal-mass components captures with the same efficiency (to within 10%) as either  $m_1$  or  $m_2$ . This is strong validation of the impulse approximation. This sort of scaling requires, of course, that the binary be split and therefore applies only to our 1C and

2C-IND results. By contrast, undisrupted binaries (2C-BIN) behave as single objects and have a capture efficiency that is independent of mass.

The impulse approximation allows us to make other predictions as well. For example, we can reverse the above scenario and predict the capture rates of two equal-mass binaries corresponding to one unequal-mass pair for which the capture rates of each component are known.

Further, given the capture rate for a single equal-mass binary, we can predict the capture efficiency of one component of an unequal-mass pair, if one parameter of the unequal-mass binary ( $m_1$ ,  $m_2$ ,  $m_1 + m_2$ , or  $a_B$ ) is set. This means that each equal-mass pair matches to a whole family of unequal-mass binaries.

Finally, we can extend these techniques to guide large-scale simulations. Using the impulse approximation, and given equal-mass capture statistics for all combinations of relevant masses and separations, we can predict the capture rates for *all* unequal-mass binaries – with any mass ratio, total mass, and separation. Similarly, knowledge of unequal-mass capture rates for one component of a binary with a fixed mass ratio allows us to estimate the capture efficiencies of *all* equal-mass binaries.

Scaling with the impulse approximation is a powerful way to predict capture rates. Practically speaking, it means that capture of any unequal-mass binaries can be predicted by studying just equal-mass cases, and accordingly, we have restricted our numerical studies to binaries with equal masses.

#### 4.6. Jupiter’s eccentricity

Most scenarios, including our own, propose that irregular satellite capture occurred early in the Solar System’s history (Section 1.1). It is likely that Jupiter’s eccentricity was closer to zero at this time and its current value was obtained later. Thus we have chosen to use  $e_J = 0$  in our simulations and believe it is a reasonable assumption.

How would Jupiter’s current eccentricity affect capture? It is not straightforward to extend this study to a non-zero jovian eccentricity for the primary reason that the Jacobi constant is no longer a constant of the motion. Though Jupiter’s current eccentricity is small ( $e_J \sim 0.048$ ), it causes the calculated  $C_J$  of an interloper to vary by  $\sim 0.2$  over an orbit. This is a variation about ten times larger than our entire range of tested Jacobi constants. Thus we cannot simply assign an initial  $C_J$  to binaries or single objects approaching an eccentric Jupiter and compare the capture results with the equivalent circular case. Only for eccentricities less than a hundredth of Jupiter’s would the errors introduced in the Jacobi constant be acceptable.

The results of Astakhov & Farrelly (2004) suggest an order of magnitude lower capture probability for single objects in the eccentric case as compared to capture by a planet orbiting on a circle. However, their initial conditions were generated using the same Jacobi constant values in the eccentric and the non-eccentric cases. Because of the variation in  $C_J$  induced by eccentricity, their method actually produces a much larger range of Jacobi constants (and much higher approach speeds) for tests with an eccentric planet, and the results should not

be directly compared with the circular case. We believe their conclusions give artificially low eccentric-case capture rates for this reason.

We do not expect Jupiter’s eccentricity to strongly affect capture. As the timescale for capture is much shorter than Jupiter’s orbital period, the planet’s instantaneous location is the most relevant factor. At pericenter, Jupiter’s Hill sphere is slightly smaller than at its average distance from the Sun and encounter speeds are slightly higher, likely resulting in fewer captures. The opposite can be expected at apocenter, causing the effects of eccentricity to average out and probably produce little change in overall capture statistics. To truly know the effects of the planet’s eccentricity would require large-scale integrations with the interlopers originating on heliocentric orbits. This is beyond the scope of our current work, but again, we suspect the difference in capture rates will be small.

#### 4.7. Survivability of captured objects

The post-capture orbits are initially very irregular and prone to collisions with Jupiter’s Galilean satellites (particularly its outermost, Callisto) or the planet itself. Figure 11 displays the percent of captured bodies that are delivered onto orbits that do not cross Callisto, which orbits Jupiter at  $26 R_J$ .

An interesting feature is the lack of any captures without close approaches for  $C_J = 3.02$  and  $3.025$ . These Jacobi constants correspond to orbital inclinations near  $90^\circ$  (see Section 4.1), where the Kozai effect is strongest. The Kozai mechanism causes the orbits to

become highly eccentric and subject to collision with Jupiter or one of the Galilean satellites. This is the primary reason that no existing satellites in the Solar System have inclinations near  $90^\circ$ .

All of the surviving binaries plotted here capture as 2C-BIN (though not all 2C-BIN captures are survivors), largely because of the separations we have studied. The separations of these binaries are optimized to give maximum capture percentages, leading to tidal disruption radii that are very close to Jupiter (Eq. 1). Thus these surviving binaries, which by definition have closest approaches outside Callisto, do not cross  $r_{td}$  and remain intact. The separations we have used, which are optimal for capture, do not correspond with the maximum survival rate. Somewhat larger separations would result in a higher percent of surviving captures, with a lower percent of overall captures.

The consequences of this are apparent in Figure 11. For  $C_J < 3.02$ , the curves for single objects and all three binary masses are equivalent to within the error. This is because most of the binary captures in this  $C_J$  range are 2C-BIN. Since 2C-BIN captures act as a single entity with no alteration from tidal disruption, the captured population for  $C_J < 3.02$  is similar to that of the single bodies and the fraction that avoid Callisto is also similar. While the surviving binaries for  $C_J > 3.025$  are still all 2C-BIN, 1C captures dominate the 2C-BIN captures in this Jacobi constant range, but none of the 1C captures are safe from Callisto. Therefore, the percent of the total binary captures that survive at high Jacobi constants is very small.

Thus we find that while retrograde captures (low  $C_J$ ) are rare (see Fig. 7), most of them are safe from collision with Callisto. On the contrary, prograde captures from binaries (high  $C_J$ ) are numerous but prone to collision. This is bad news for binary capture – the largest enhancements occur for captures that are most likely to be removed by interactions with Callisto. As we have already discussed, examining larger separations will lead to a larger percentage of capture orbits that are safe from collision. This may be a significant effect. How else can collisions be avoided?

One possible way out is if the captures occurred before Callisto was formed. At these early times, a dense accretion disk surrounded Jupiter, and the strong gas drag could have augmented capture rates (as in Pollack *et al.*, 1979). However, this is not compelling, because satellites captured at this time would be prone to loss by orbital decay and later by collisions with forming proto-satellites.

The most likely mechanism for preventing captured bodies from colliding is gas drag from the remaining gas present outside Callisto’s orbit at the time of capture. A small amount of gas is necessary for our mechanism in order to shrink capture orbits to their current sizes. This process can also increase the pericenters of the captured objects, causing them to avoid collision with Callisto. A typical collision timescale for a Callisto-crossing orbit with  $a = 0.5r_H$  and  $i = 10^\circ$  is on the order of  $10^6$  years, long enough for gas to evolve the satellites onto safe orbits (see Section 1.2). The timescale is longer for more tilted orbits, but significantly shorter for retrograde orbits.

A tenuous gas around Jupiter and Saturn near the end of planet formation is consistent with our current understanding of planet formation (Section 1.2). If gas was present at the time of capture, its structure and density are not well constrained, and thus we do not focus on the orbital evolution process itself in this work. As a simple example, however, we simulated a drag force that acts against the velocity vector and show that it is able to both shrink the post-capture orbits and prevent the new satellites from collision. In Fig. 12, we plot the initial and final states for a prograde and retrograde orbit. The gas drag is applied after capture for simplicity; this is valid because the timescale for temporary capture is  $\sim$ months, and the effects of the gas are negligible over such a short time. The final states are chosen so that the orbits lie approximately where the current progrades and retrogrades orbit at Jupiter (at  $\sim \frac{1}{4}r_H$  and  $\sim \frac{1}{2}r_H$ , respectively), and they have pericenters outside Callisto’s orbit. The drag strengths were set so that the evolution for both orbits occurs over 25,000 years. However, with a more tenuous gas than in this example, the same evolution could take place on timescales 10-100 times longer. The binary capture mechanism discussed here constrains only the amount of orbital evolution, not the evolution rate, and hence avoids the satellite loss problem of capture-by-gas-drag models.

## 5. Discussion

The new model discussed here, capture from low-mass binaries with subsequent orbital evolution, has both significant advantages and disadvantages in comparison to other

suggested models.

One important advantage is that capture is viable at Jupiter and Saturn, unlike three of the models discussed in Section 1. For example, Agnor & Hamilton’s (2006) direct three-body capture model works only for very large bodies in the gas giants’ high-approach-speed environments. Also, the theory of Nesvorný *et al.* (2003) requires close approaches among the giant planets, of which Jupiter has very few in the Nice model scenario. Saturn encounters its outer neighbors more frequently than Jupiter, but it still suffers from few close approaches overall in this model. In Vokrouhlický *et al.* (2007), the capture statistics from planet-binary encounters are low for all planets, but especially Jupiter and Saturn. This is primarily because of the high relative velocities assumed in their model. Though these latter two capture mechanisms in their current forms cannot explain the gas giants’ irregular satellites, they are worth further study, perhaps in the context of altered versions of the Nice model or other early Solar System models.

Our model also has an important advantage over that of Pollack *et al.*, 1979, in that our capture scenario allows for a much weaker gas, since the gas here is needed for shrinking the orbits, not capturing satellites. Also, the gas in our model can persist for much longer than that in Pollack *et al.*, as a weaker gas does not have the problem of quickly destroying the captured bodies. Furthermore, various groups (e.g., Canup & Ward, 2002) have proposed that the Galilean satellites formed from a tenuous gas; if true, the gas was most likely even thinner when the irregular satellites were captured. Thus it is important that our capture

mechanism does not rely on a dense gas.

To directly compare our mechanism with that of Astakhov *et al.* (2003), we need to consider both relative capture rates (and their survivability) and the prevalence of binaries vs. single bodies. In our simulations, we find that binary capture can provide a significant advantage over capturing from populations of single bodies for binaries with particular characteristics: high enough masses ( $\gtrsim 100$  km), optimal separations ( $\sim 10\text{-}20 R_B$ ), and low incoming energies (corresponding to Jacobi constants  $\gtrsim 3.02$  and mostly prograde encounters). However, like Astakhov *et al.* (2003), we also find that the probability of captures (from either binaries or single bodies) of avoiding collisions with Callisto is low for readily captured progenitors. In Section 4.7, we discussed that this problem can be alleviated by altering the capture orbits with the surrounding gas or by capturing binaries with larger-than-optimal separations that do not lead to Callisto-crossing orbits.

So, how common were easily-captured binaries early in Solar System history? This question is difficult to assess. Observational surveys of the current population of the cold, classical Kuiper belt (i.e. objects with modest inclinations and eccentricities) find a 30% binary fraction among bodies larger than 100 km (Noll *et al.*, 2008), many with nearly equal mass components. Also, recent studies of planetesimal formation have suggested that large,  $\gtrsim 100$ -km bodies may form quickly in the gaseous proto-planetary disk, providing the building blocks of subsequent planet formation (Johansen *et al.*, 2007; Cuzzi *et al.*, 2008). Binary formation is likely to be contemporaneous with the formation of these bodies

(Nesvorný, 2008). Further, Morbidelli *et al.* (2009) have shown that the size-frequency distribution of asteroids in the main belt is consistent with large initial planetesimals, at least  $\sim 100$ -km in size. Together these results indicate that the  $\sim 100$ -km binary objects considered here may have been quite common as the very last portions of the Solar System’s gas disk were being depleted.

Finally, the known irregular satellite population numbers  $< 100$ , and many of these are probably members of families – thus, we need only produce at most a few dozen captures. While accounting for the origin of such a small population is difficult, our simulations show that it is likely binaries played a role. We conclude by offering our model as a new idea that alleviates many but not all of the problems faced by previous models, but acknowledge that the without a detailed understanding of the initial population including binary statistics, a firm conclusion is not possible.

## REFERENCES

- Agnor, C. B. and Hamilton, D. P., 2006a. Neptune’s capture of its moon Triton in a binary-planet gravitational encounter. *Nature* 441, 192-194.
- Agnor, C. B. and Hamilton, D. P., 2006b. Satellite capture via binary-planet gravitational encounters. *Bull. Am. Astron. Soc.* 38, 674.
- Astakhov, S. A. and Farrelly, D., 2004. Capture and escape in the elliptic restricted three-body problem. *Mon. Not. R. Astron. Soc.* 354, 971-979.
- Astakhov, S. A., Burbanks, A. D., Wiggins, S., and Farrelly, D., 2003. Chaos-assisted capture of irregular moons. *Nature* 423, 264-267
- Bate, M. R., Lubow, S. H., Ogilvie, G. I., and Miller, K. A., 2003. Three-dimensional calculations of high- and low-mass planets embedded in protoplanetary discs. *Mon. Not. R. Astron. Soc.* 341, 213-229.
- Canup, R. M. and Ward, W. R., 2002. Formation of the Galilean satellites: Conditions of accretion. *Astron. J.* 124, 3404-3423.
- Cieza, L. and 19 colleagues, 2007. The Spitzer c2d survey of weak-line T Tauri stars. II. New constraints on the timescale for planet building. *Astrophys. J.* 667, 308-328.
- Colombo, G. and Franklin, F. A., 1971. On the formation of the outer satellite groups of Jupiter. *Icarus* 15, 186-189.

- Ćuk, M. and Burns, J. A., 2004a. Gas-drag-assisted capture of Himalia’s family. *Icarus* 167, 369-381.
- Ćuk, M. and Burns, J. A., 2004b. On the secular behavior of irregular satellites. *Astron. J.* 128, 2518-2541.
- Cuzzi, J. N., Hogan, R. C., and Shariff, K., 2008. Toward planetesimals: Dense chondrule clumps in the protoplanetary nebula. *Astrophys. J.* 687, 1432-1447.
- D’Angelo, G., Henning, T., and Kley, W., 2003. Thermohydrodynamics of circumstellar disks with high-mass planets. *Astrophys. J.* 599, 548-576.
- Hamilton, D. P. and Burns, J. A., 1991. Orbital stability zones about asteroids. *Icarus* 92, 118-131.
- Henon, M., 1969. Numerical exploration of the restricted problem, V. *Astron. Astrophys.* 1, 223-238.
- Heppenheimer, T. A. and Porco, C., 1977. New contributions to the problem of capture. *Icarus* 30, 385-401.
- Jewitt, D. and Sheppard, S., 2005. Irregular satellites in the context of planet formation. *Space Science Reviews* 116, 441-455.
- Johansen, A., Oishi, J. S., Low, M.-M. M., Klahr, H., Henning, T., and Youdin, A., 2007. Rapid planetesimal formation in turbulent circumstellar disks. *Nature* 448, 1022-1025.

- Lubow, S. H., Seibert, M., and Artymowicz, P., 1999. Disk accretion onto high-mass planets. *Astrophys. J.* 526, 1001-1012.
- Merline, W. J. and 11 colleagues, 2007. The search for Trojan binaries. *Bull. Am. Astron. Soc.* 38, 538.
- Morbidelli, A., Bottke, W. F., Nesvorný, D., and Levison, H. F., 2009. Asteroids were born big. *Icarus*, in press.
- Mosqueira, I. and Estrada, P. R., 2003. Formation of the regular satellites of giant planets in an extended gaseous nebula I: Subnebula model and accretion of satellites. *Icarus* 163, 198-231.
- Murray, C. D. and Dermott, S. F., 1999. *Solar System Dynamics*. Cambridge Univ. Press, Cambridge, UK.
- Nesvorný, D., 2008. Formation of Kuiper belt binaries. *Bull. Am. Astron. Soc.* 40, 464.
- Nesvorný, D., Alvarellos, J. L. A., Dones, L., and Levison, H. F., 2003. Orbital and collisional evolution of the irregular satellites. *Astron. J.* 126, 398-429.
- Nesvorný, D., Vokrouhlický, D., and Morbidelli, A., 2007. Capture of irregular satellites during planetary encounters. *Astron. J.* 133, 1962-1976.
- Noll, K. S., Grundy, W. M., Stephens, D. C., Levison, H. F., Kern, S. D., 2008. Evidence for two populations of classical transneptunian objects: The strong inclination dependence of classical binaries. *Icarus* 194, 758-768.

- Papaloizou, J. C. B., Nelson, R. P., Kley, W., Masset, F. S., and Artymowicz, P., 2007. Disk-planet interactions during planet formation. In: Reipurth, D., Jewitt, D., and Keil, K. (Eds.), *Protostars and Planets V*, Univ. of Arizona Press, Tucson, 655-668.
- Pollack, J. B., Burns, J. A., and Tauber, M. E., 1979. Gas drag in primordial circumplanetary envelopes – a mechanism for satellite capture. *Icarus* 37, 587-611.
- Pollack, J. B., Hubickyj, O., Bodenheimer, P., Lissauer, J. J., Podolak, M., and Greenzweig, Y., 1996. Formation of the giant planets by concurrent accretion of solids and gas. *Icarus* 124, 62-85.
- Rauch, K. P. and Hamilton, D. P., 2002. The HNBODY package for symplectic integration of nearly-Keplerian systems. *Bull. Am. Astron. Soc.* 34, 938.
- Saha, P. and Tremaine, S., 1993. The orbits of the retrograde Jovian satellites. *Icarus* 106, 549-562.
- Sheppard, S. S. and Jewitt, D. C., 2003. An abundant population of small irregular satellites around Jupiter. *Nature* 423, 261-263.
- Silverstone, M. D. and 16 colleagues, 2006. Formation and Evolution of Planetary Systems (FEPS): Primordial warm dust evolution from 3 to 30 Myr around Sun-like stars. *Astrophys. J.* 639, 1138-1146.
- Strutskie, M. F., Dutkevitch, D., Strom, S. E., Edwards, S., Strom, K. M., and Shure,

M. A., 1990. A sensitive 10-micron search for emission arising from circumstellar dust associated with solar-type pre-main-sequence stars. *Astron. J.* 99, 1187-1195.

Tsiganis, K., Gomes, R., Morbidelli, A., and Levison, H. F., 2005. Origin of the orbital architecture of the giant planets of the Solar System. *Nature* 435, 459-461.

Whipple, A. L. and Shelus, P. J., 1993. A secular resonance between Jupiter and its eighth satellite? *Icarus* 101, 265-271.

Vokrouhlický, D., Nesvorný, D., and Levison, H. F., 2008. Irregular satellite capture by exchange reactions. *Astron. J.* 136, 1463-1476.

Table 1. Mass Ratio Tests For Binaries With  $C_J=3.03$

Mass Ratio	Component Radii (km)	Total Binary Mass ( $10^{19}$ kg)	Separation (km)	$m_1$ Capture Percentage	$m_2$ Capture Percentage	Total 1C Capture Percentage
3:2	113-98	2.0	1350	<b>0.54</b>	<i>0.96</i>	1.50
1:1	85-85	1.0	1080	<b>0.58</b>	<b>0.58</b>	1.16
1:1	127-127	3.4	1620	<i>0.94</i>	<i>0.94</i>	1.88
4:1	124-78	2.0	1160	<b>0.21</b>	<i>1.17</i>	1.38
1:1	42-42	0.13	465	<b>0.24</b>	<b>0.24</b>	0.48
1:1	169-169	8.1	1860	<i>1.29</i>	<i>1.29</i>	2.58

Note. — Two experiments with binaries of unequal mass. The first four columns identify properties of the binary, while the final three columns list capture statistics (with  $m_1 \geq m_2$ ). We used the impulse approximation (Eqs. 1 and 2) to determine the properties of equivalent equal-mass binaries that match the tidal disruption radius and speed of either  $m_1$  (boldfaced) or  $m_2$  (italicized). In all cases, our predicted percentages agree with the actual measurements to within about 10%.

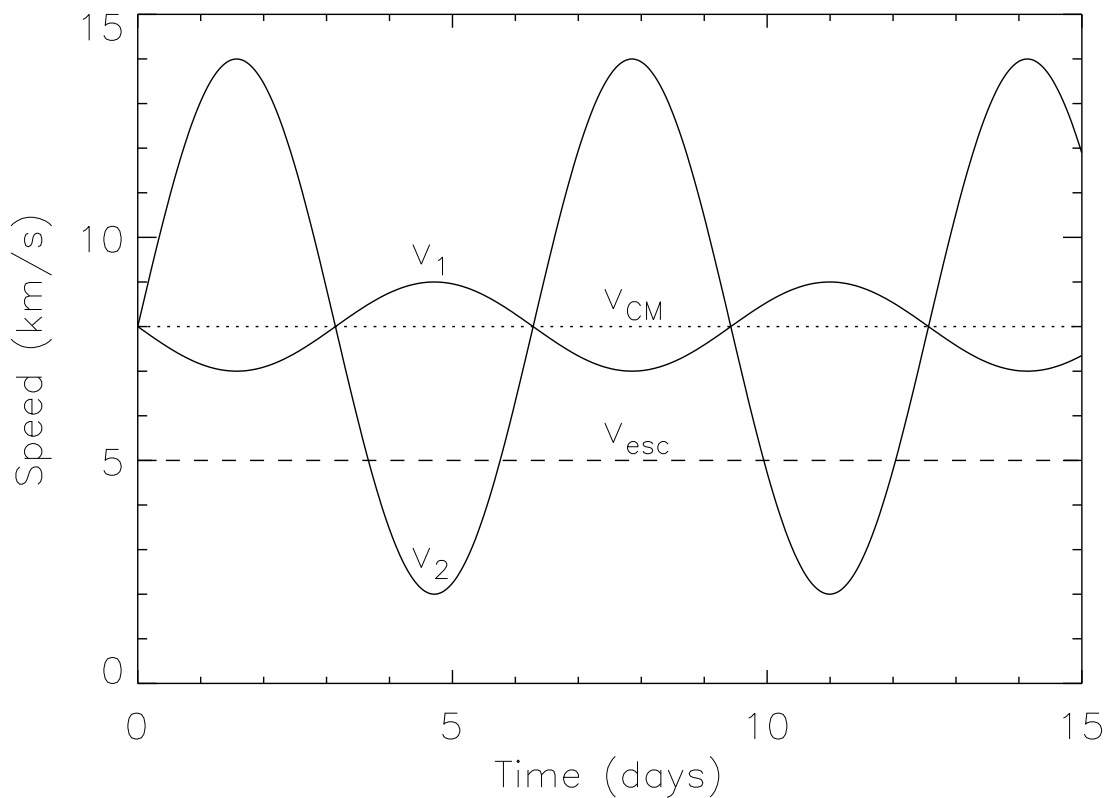


Fig. 1.— The speeds of unequal-mass binary components ( $v_1$  and  $v_2$ ) and the center-of-mass speed ( $v_{CM}$ ) relative to Jupiter, where  $m_1 > m_2$ . Since the binary center of mass approaches the planet along a hyperbolic trajectory, it is always traveling faster than the escape speed ( $v_{esc}$ ). In this example, the smaller component’s speed dips below the escape speed for a portion of its orbit. If the binary is disrupted during this interval, the smaller component will be captured by the planet.

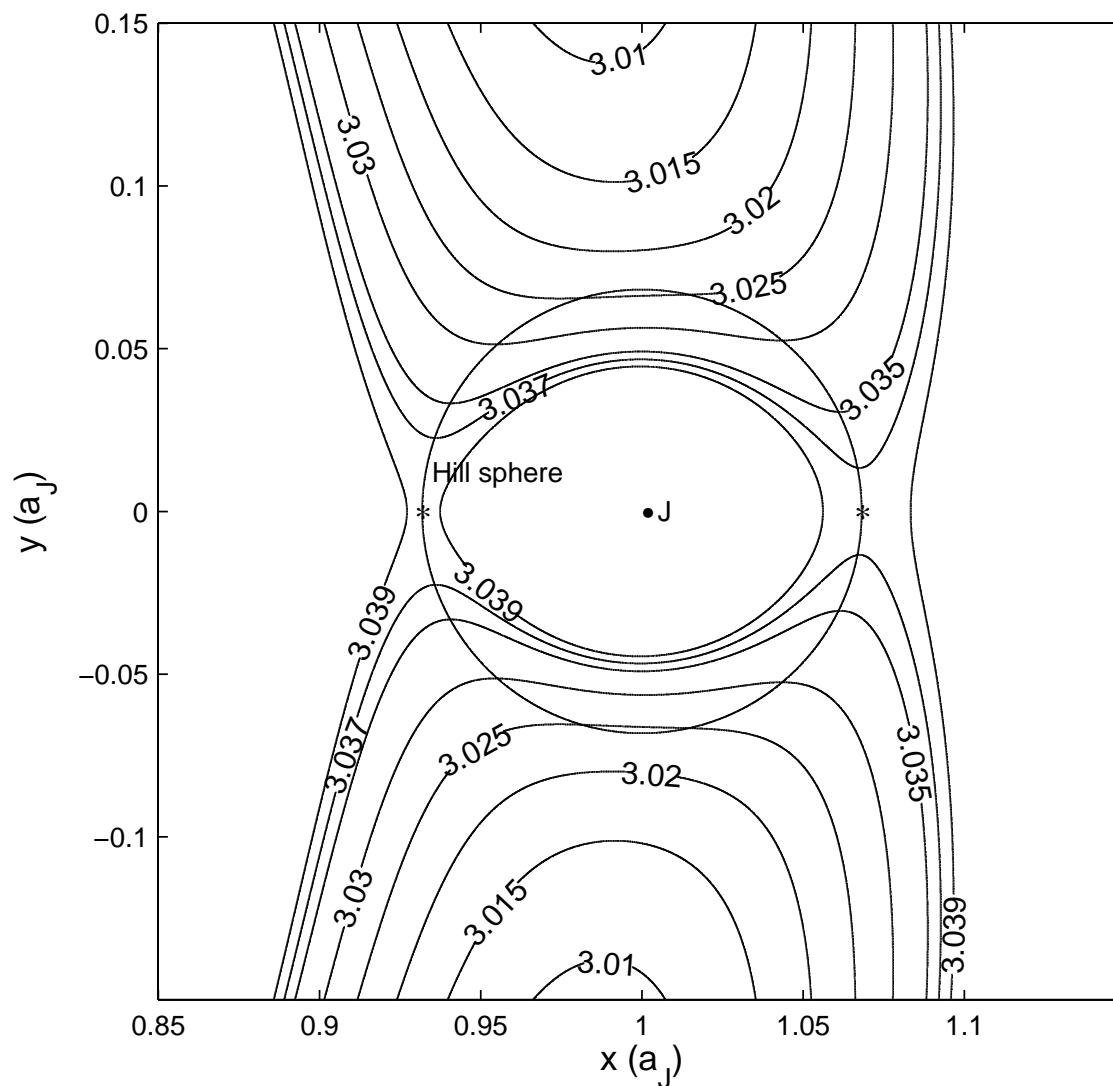


Fig. 2.— The Hill sphere of Jupiter (central dot marked 'J') with zero-velocity curves (ZVCs) corresponding to the labeled Jacobi constant ( $C_J$ ) values. The Sun is to the left at (0,0) and the Jupiter-Sun separation ( $a_J$ ) is used as the unit of distance. The two asterisks are located at the planet's  $L_1$  and  $L_2$  Lagrange points. A body near Jupiter with  $C_J \gtrsim 3.0387$  (e.g., the curve for  $C_J = 3.039$ ) has ZVCs enclosed around the planet, and it would be unable to escape.

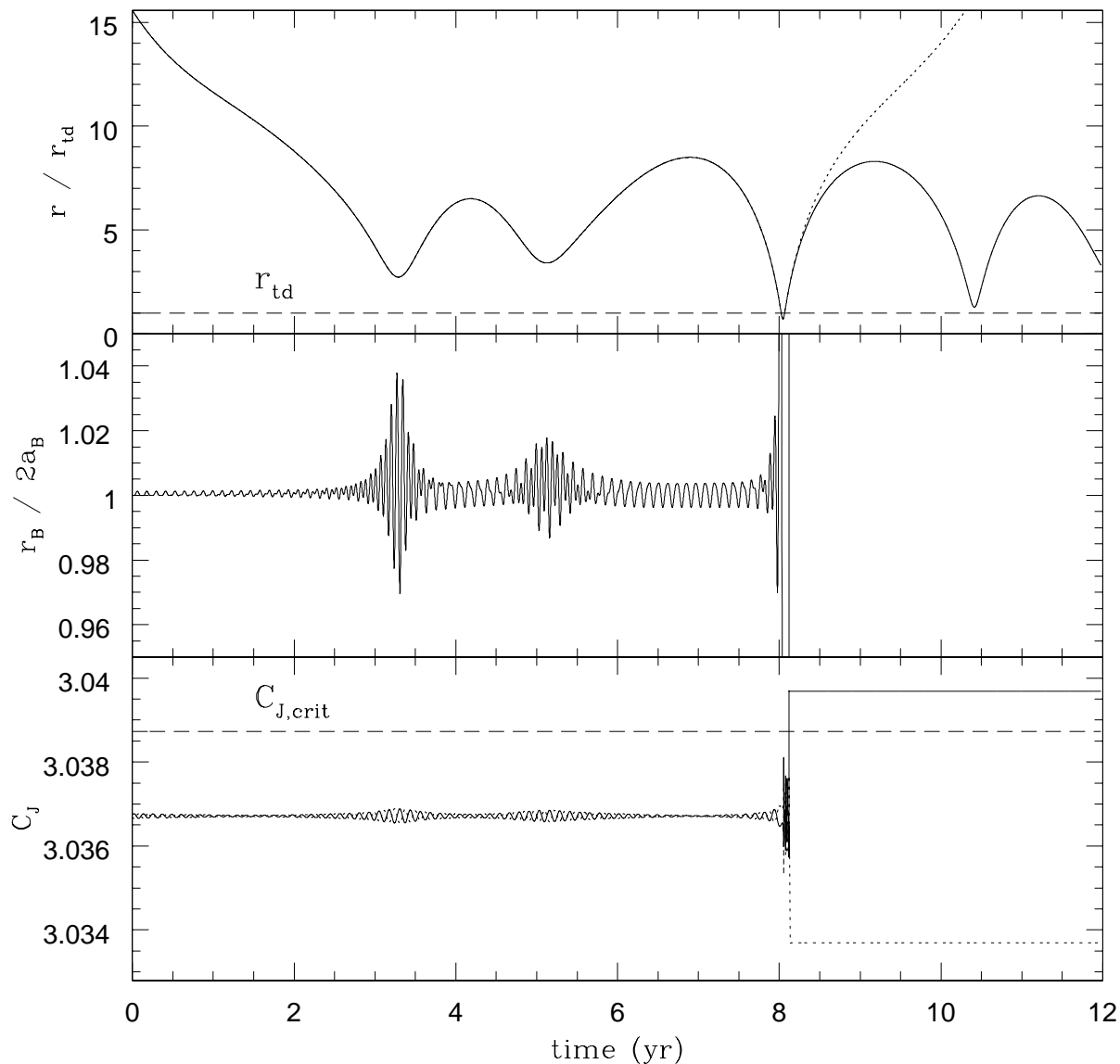


Fig. 3.— Distance from the binary components (each 65-km in radius) to Jupiter ( $r$ ) is plotted in units of the tidal disruption radius ( $r_{td} \approx 70 R_J$ ) in the top panel; the middle panel shows the binary’s separation ( $r_B$ ) over time, in units of its initial separation ( $2a_B$ ); and the bottom panel displays the Jacobi constant of each component. One component is plotted with a solid line and the other with a dotted line throughout the figure. The dashed line in the top panel indicates the tidal disruption radius. In the bottom panel, the dashed line represents the critical Jacobi constant.

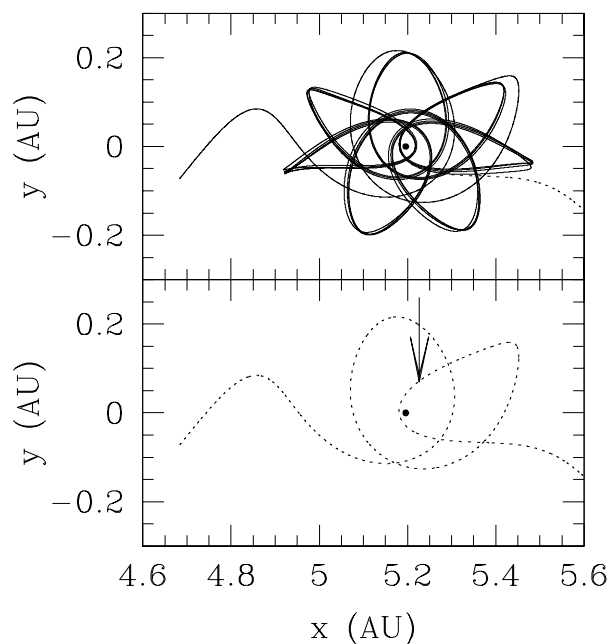


Fig. 4.— The orbits of the binary components discussed in Fig. 3. Jupiter is the dot near the center of each panel, and the Sun is located to the left at (0,0). The components are plotted together in the top panel, with solid/dotted lines corresponding to those in Fig. 3. The objects are bound to each other as they approach Jupiter from the left side of each panel. A close approach to the planet tidally disrupts the binary, sending one component (dotted line) out of the system and causing the other component (solid line) to be permanently captured by the planet. The bottom panel contains only the orbit of the component that escapes, with an arrow marking the location where the binary’s separation first exceeds 102% of its original value. About equidistant on the other side of the planet, the binary’s separation is more than twice its initial value.

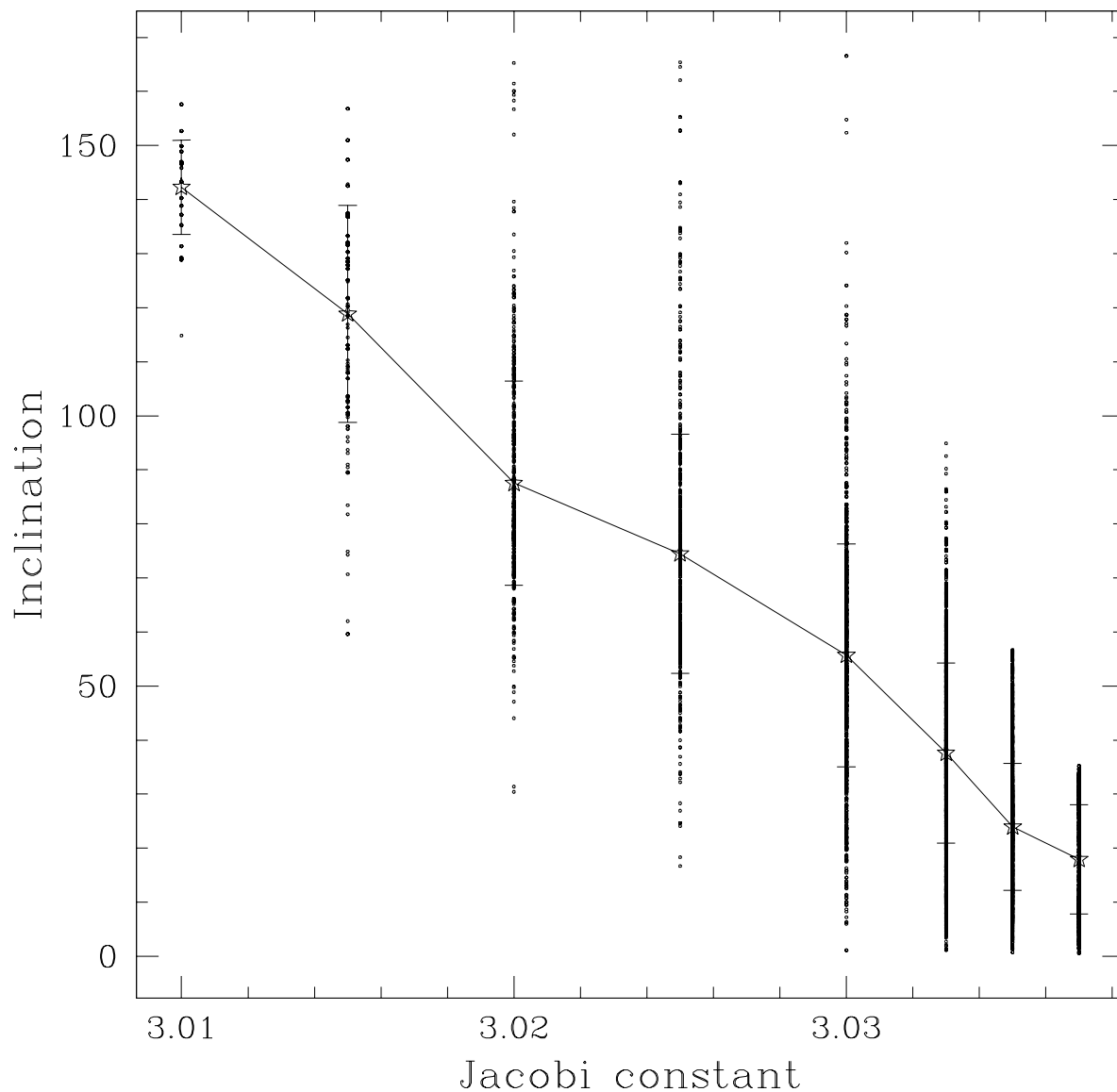


Fig. 5.— Inclination of 100-km captured binary components as a function of initial Jacobi constant, plotted for the bodies’ first close approaches. Similar plots show that the relationship holds for all close approaches of binaries or single bodies, captured or not. Also plotted is a line connecting the mean at each Jacobi constant (marked by the stars) as well as 1- $\sigma$  error bars. See Section 4.1 for discussion on the  $C_J$ -inclination relationship.

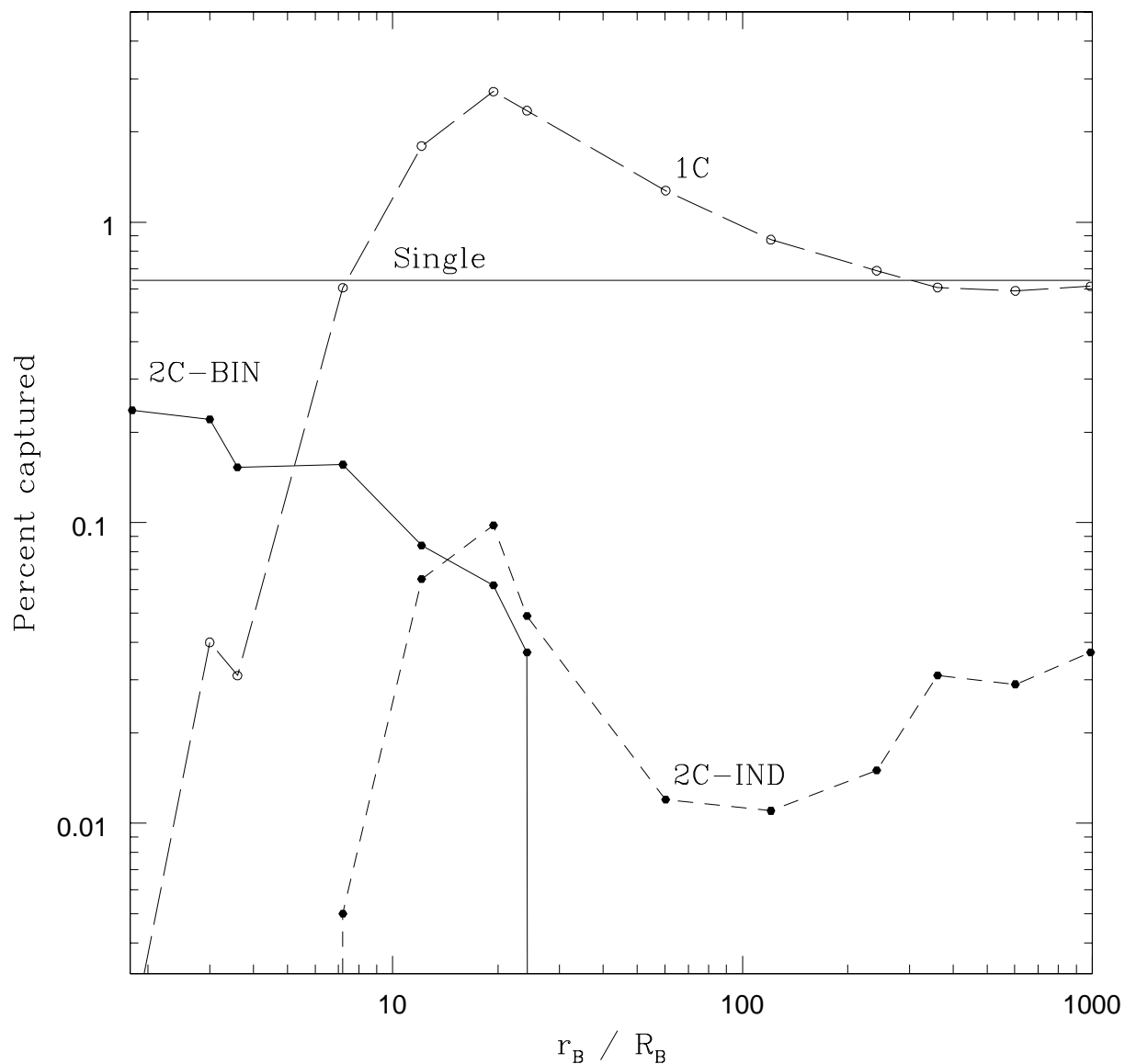


Fig. 6.— Three modes of capture for integrations of  $R_B = 65$ -km binary pairs with  $C_J = 3.037$ , as a function of the separation of the binary ( $r_B$ ): one component captures ('1C'), the binary splits and both capture independently ('2C-IND'), or the binary remains bound and captures as a pair ('2C-BIN'). We plot the capture percentage for objects (rather than binaries) to facilitate comparison with single bodies (upper solid line). Recall our working definition of capture to mean bodies still orbiting the planet after 1,000 years. Note that the 2C-BIN curve approaches the value for singles at small separations while the sum of the 1C and 2C-IND captures rates approaches the same value for large separations.

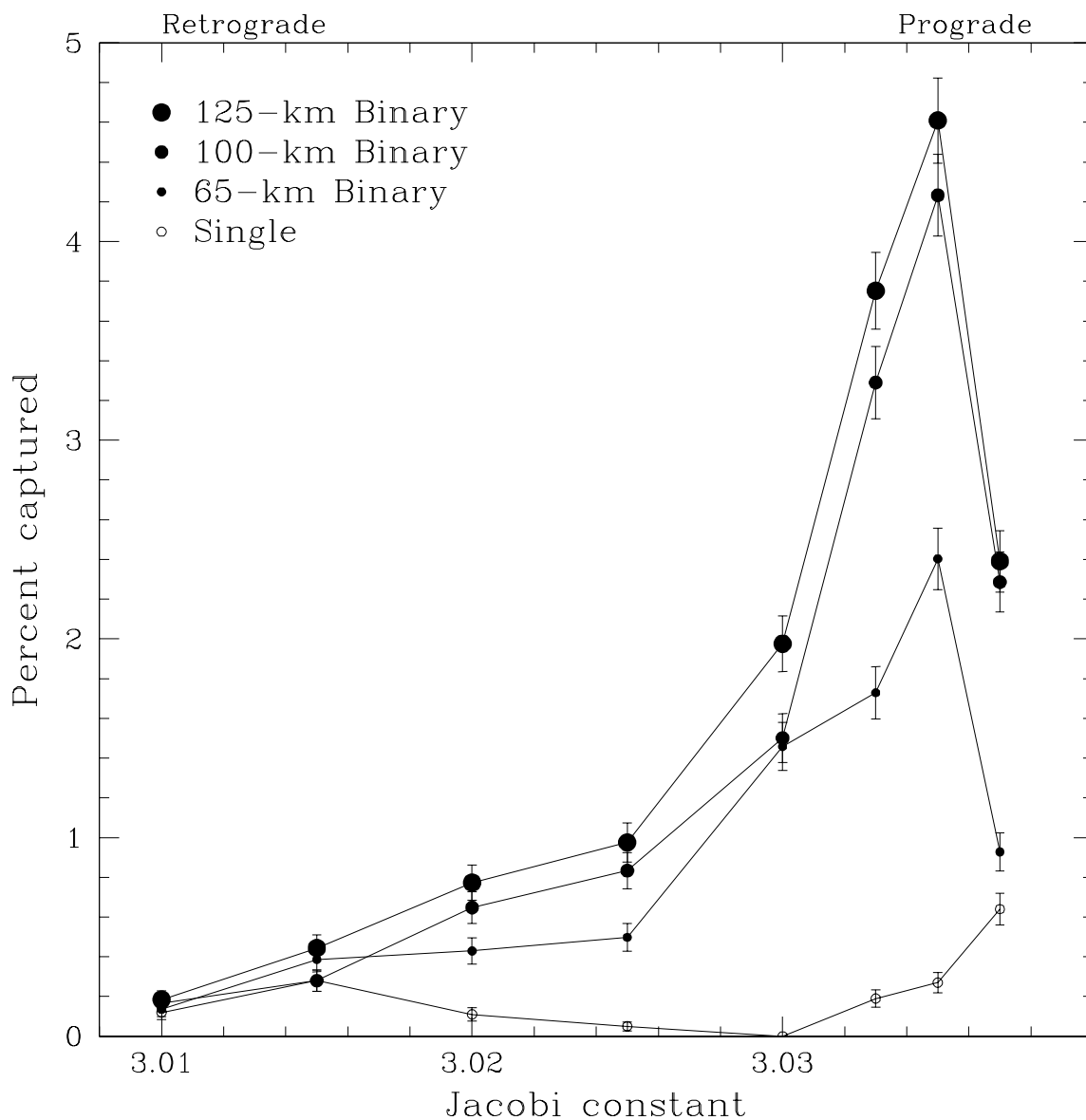


Fig. 7.— Capture percentages for binaries of different masses compared to single objects. All bodies were started on Jupiter’s Hill sphere. For each binary mass, a single separation was used over the range of initial Jacobi constants: 471 km = 7.25 binary radii ( $R_B$ ) for the 65-km binaries, 1225 km = 12.25  $R_B$  for the 100-km set, and 1512 km = 12.10  $R_B$  for 125-km binaries. These separations give near maximum capture rates for the majority of the Jacobi constants tested, with the exception of the highest  $C_J$ , where the optimum separation is closer to 20 binary radii.

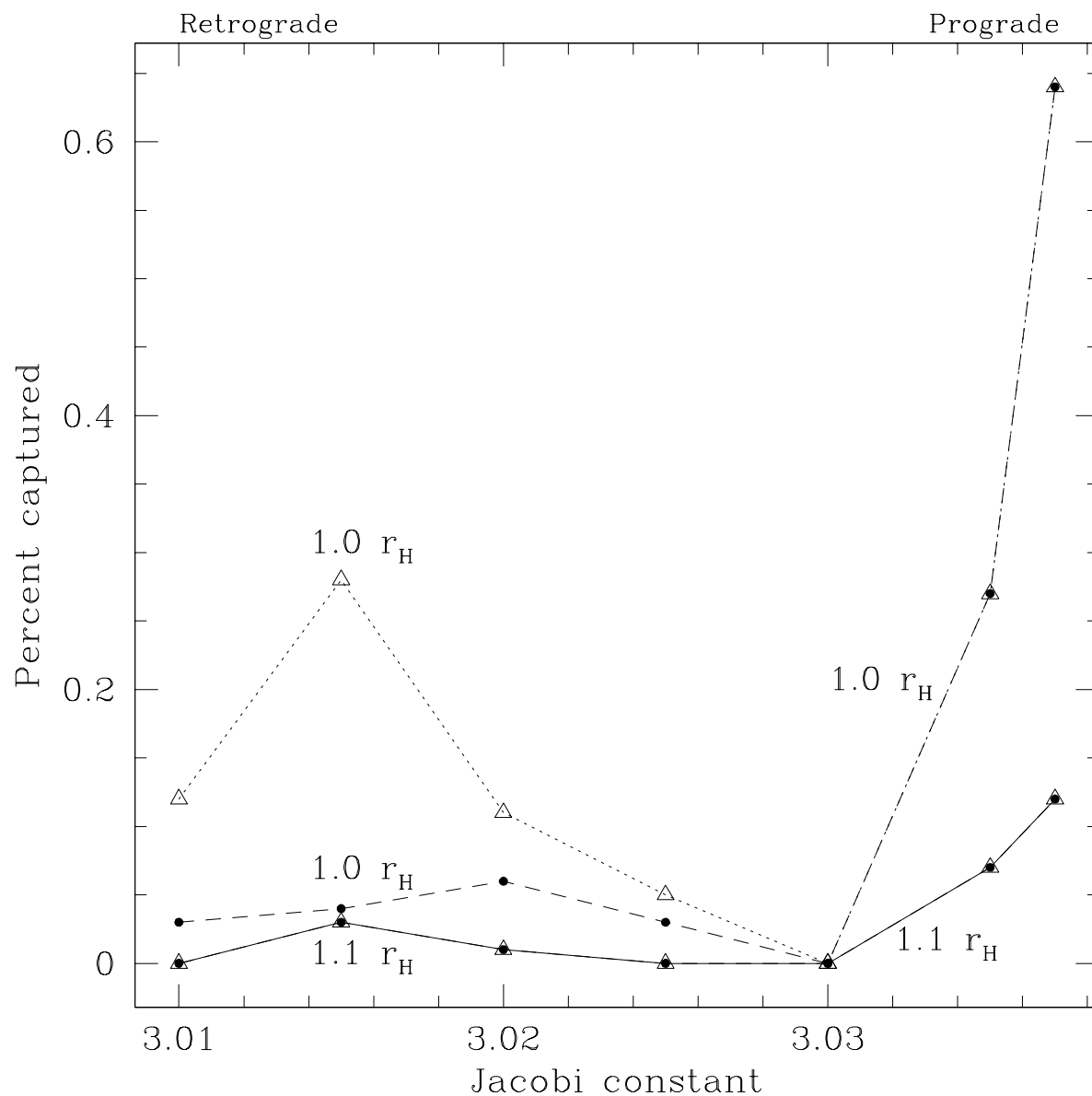


Fig. 8.— Single objects integrated from two launch distances. True captures curves (with points that are solid circles) show only those captures that originated far from Jupiter, while curves that show true plus contaminated captures (with open triangles) also include objects that were stably orbiting the planet at the beginning of the integrations. For launch on the Hill sphere ( $1.0 r_H$ ), we see that the prograde orbits (high  $C_J$ ) are not affected at all, while many of the retrograde orbits (low  $C_J$ ) are discovered to be false. For launches at  $1.1 r_H$ , the true and true-plus-contaminated curves overlap completely, showing that contamination by false captures is effectively zero.

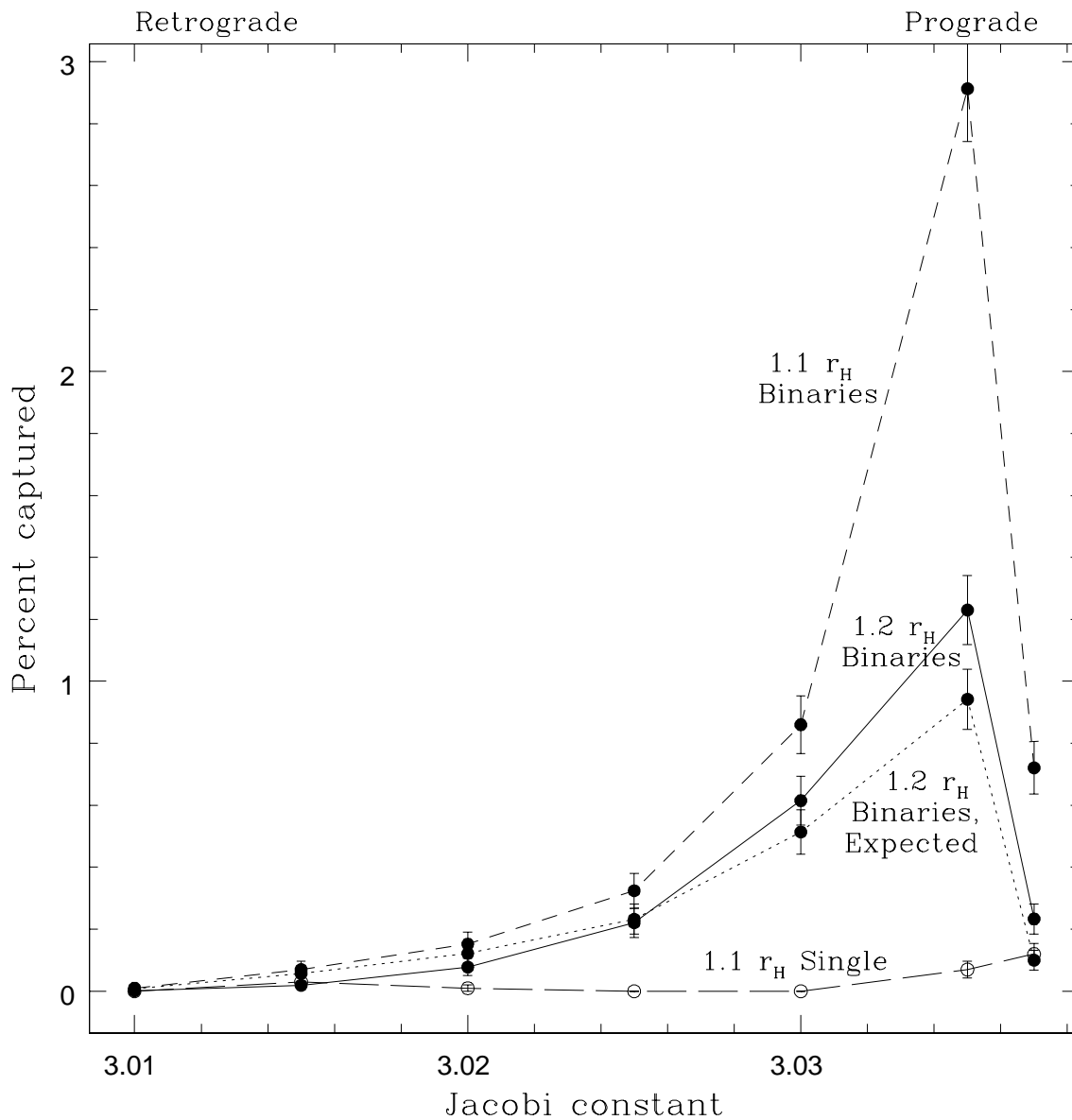


Fig. 9.— Capture rates of 100-km binaries that were launched from  $1.1 r_H$  (upper dashed line),  $1.2 r_H$  (solid line), and expected capture rates for  $1.2 r_H$  (dotted line) calculated by scaling the  $1.1 r_H$  rates by the percent of  $1.2 r_H$  trajectories crossing interior to the  $1.1$  Hill radii. All are shown with  $1\text{-}\sigma$  error bars. This scaling equalizes the capture percentages between the two launch distances to within 20%. For reference, the capture rate for single bodies starting from  $1.1 r_H$  is also plotted; compare with Fig. 7.

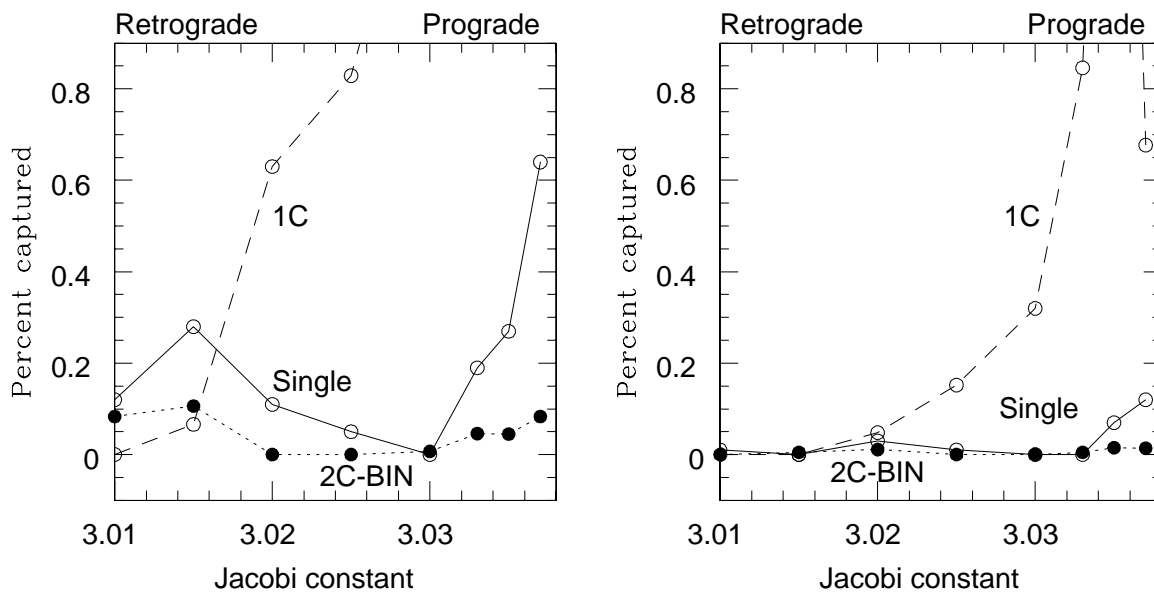


Fig. 10.— Modes of capture vs. Jacobi constant, for integrations of 100-km binaries starting at  $1.0 r_H$  (left panel) and  $1.1 r_H$  (right panel). The 1C curve peaks are off the top of the plot at  $\sim 4.2\%$  for the  $1.0 r_H$  runs and  $\sim 3.0\%$  for the  $1.1 r_H$  group. The 2C-IND capture rates are extremely small for both starting distances (e.g., Fig. 6) and, for clarity, are not plotted here. The capture rates of single bodies are plotted for comparison.

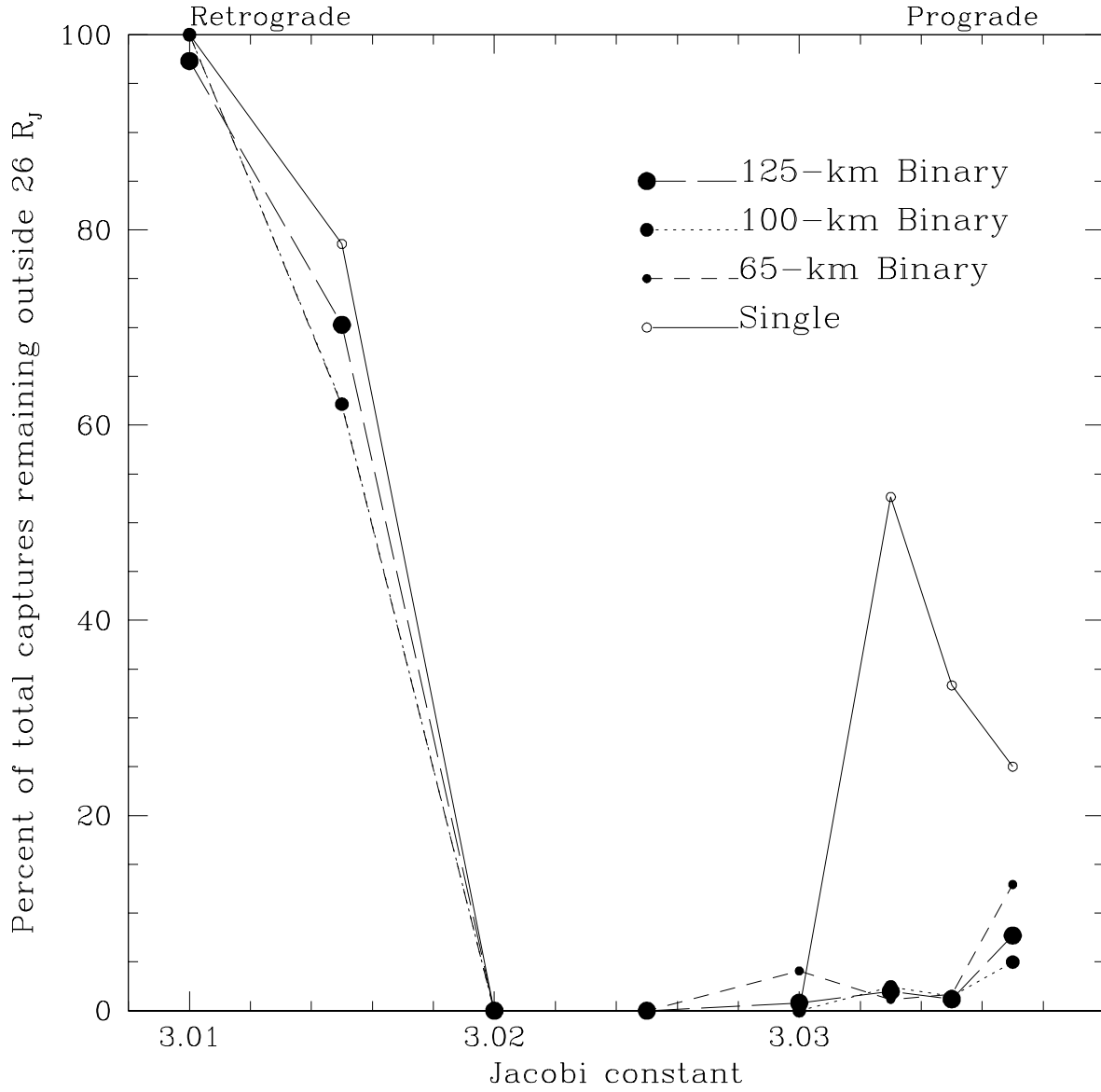


Fig. 11.— The percent of captured objects that do not cross interior to 26  $R_J$  (Callisto's semi-major axis) during the 1,000-year integrations. The bodies were started on the Hill sphere. Compare with the entire set of captures seen in Fig. 7.

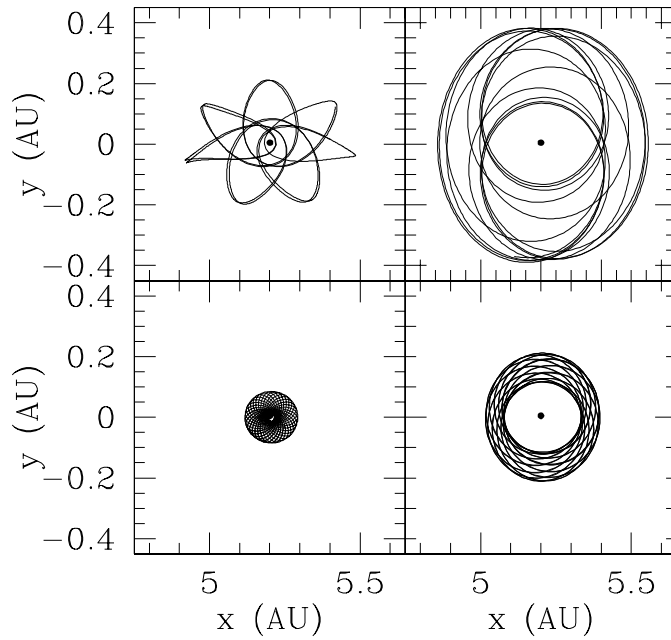


Fig. 12.— An example of a simple gas drag applied to a prograde (left panels; the same initial orbit as in Figs. 3 and 4) and a retrograde orbit (right panels). The orbits are shown immediately after capture in the upper panels, and the bottom panels show the orbits after 25,000 years of evolution. Jupiter is the dot in the center, and the Sun is to the left at (0,0). These orbits are the result of 1C capture from equal-mass binaries with 65-km components. Before disruption, the prograde binary had a separation of  $70 R_B$  and a Jacobi constant of  $\sim 3.037$ . The retrograde binary had an initial  $C_J$  of  $\sim 3.003$  and was initially separated by  $460 R_B$ .